J. Fluid Mech. (2008), *vol.* 594, *pp.* 59–69.
doi:10.1017/S0022112007009020 Printed in the United Kingdom

Coherent structures in direct numerical simulation of turbulent boundary layers at Mach 3

MATTHEW J. RINGUETTE, MINWEI WU AND M. PINO MARTÍN

Mechanical and Aerospace Engineering Department, Princeton University, Engineering Quad, Olden St, Princeton, NJ 08544, USA

(Received 15 February 2007 and in revised form 10 August 2007)

We demonstrate that data from direct numerical simulation of turbulent boundary layers at Mach 3 exhibit the same large-scale coherent structures that are found in supersonic and subsonic experiments, namely elongated, low-speed features in the logarithmic region and hairpin vortex packets. Contour plots of the streamwise mass flux show very long low-momentum structures in the logarithmic layer. These low-momentum features carry about one-third of the turbulent kinetic energy. Using Taylor's hypothesis, we find that these structures prevail and meander for very long streamwise distances. Structure lengths on the order of 100 boundary layer thicknesses are observed. Length scales obtained from correlations of the streamwise mass flux severely underpredict the extent of these structures, most likely because of their significant meandering in the spanwise direction. A hairpin-packet-finding algorithm is employed to determine the average packet properties, and we find that the Mach 3 packets are similar to those observed at subsonic conditions. A connection between the wall shear stress and hairpin packets is observed. Visualization of the instantaneous turbulence structure shows that groups of hairpin packets are frequently located above the long low-momentum structures. This finding is consistent with the very large-scale motion model of Kim & Adrian (1999).

1. Introduction

Recent laboratory and numerical experiments indicate that large-scale coherent structures play a key role in wall-bounded turbulent flows at incompressible and supersonic conditions. The majority of data come from subsonic flows. Streamwise spectra from previous pipe, channel, and boundary layer studies indicate structures in the logarithmic region with wavelengths of 10–20 boundary layer thicknesses, δ (Jiménez 1998). The pipe flow experiments of Kim & Adrian (1999) showed streamwise modes with wavelengths reaching 12–14 pipe radii, which they called very large-scale motions (VLSM) to distinguish them from $O(\delta)$ turbulent bulges. Guala, Hommema & Adrian (2006) demonstrated that these VLSM contain about half of the streamwise turbulent kinetic energy and more than half of the Reynolds shear stress, and Balakumar & Adrian (2007) reported similar structures in channel and boundary layer flows, albeit with shorter wavelengths. Recent results from large-domain direct numerical simulations (DNS) of turbulent channel flows also show long streamwise modes with wavelengths in excess of 5 channel half-widths (see del Álamo & Jiménez 2003; del Álamo *et al.* 2004). Hutchins & Marusic (2007*a*) used a spanwise rake of

10 hot-wire probes along with Taylor's hypothesis to visualize alternating low- and high-speed streamwise structures of length greater than 20δ in the logarithmic region of a turbulent boundary layer; the authors termed these features 'superstructures'. Moreover, they used a synthetic flow field to show that the spanwise meandering of the superstructures conceals their true length from single-point statistics. Hutchins & Marusic (2007*b*) also demonstrated that the superstructures have a modulating effect on the generation of small-scale near-wall motions. Adrian, Meinhart & Tomkins (2000), Tomkins & Adrian (2003), Ganapathisubramani, Longmire & Marusic (2003), and Hambleton, Hutchins & Marusic (2006) performed digital particle image velocimetry (DPIV) in turbulent boundary layers in streamwise/wall-normal or wall-parallel planes. They found evidence that the large-scale low-speed structures are created by the induced low-momentum flow from groups of vortices consistent with the hairpin packet model proposed by Adrian *et al.* (2000). We follow Adrian *et al.* (2000) and use the term 'hairpin' to refer to both symmetric or horseshoe-like vortices (as first proposed by Theodorsen 1952) and asymmetric, e.g. 'cane'-like, vortices.

The packet model states that hairpins commonly convect together in closely spaced streamwise groups, typically forming a ramp-like structure with a downstream angle relative to the wall and a maximum length of about 2δ. It offers explanations for phenomena such as the bursting event. Hairpin packets were first observed in experiments by Head & Bandyopadhyay (1981). Ganapathisubramani *et al.* (2003) found that hairpin packets and the low-speed regions induced below them contribute significantly to the Reynolds stress. Del Álamo *et al.* (2006) introduced an alternative model based on vortex 'clusters' and their wakes, which they point out is kinematically similar to the packet model but has significant dynamical differences. Here we adopt the term 'hairpin packet.' Kim & Adrian (1999) proposed that the low-momentum VLSM are the result of streamwise groups of hairpin packets having spanwise alignment such that the low-speed zones beneath them merge. Although there is no direct evidence for this VLSM model, the three-dimensional visualizations of a low-Reynolds-number turbulent boundary layer by Delo, Kelso & Smits (2004) offer an explanation for the formation of superstructures that is consistent with it. They observed groups of large-scale structures reaching 5δ in length that caused multiple ejections of the low-speed fluid below them. They proposed a growth mechanism for these 'agglomerations', consisting of a cycle of triggered ejections followed by entrainment of the ejected fluid at the trailing edge of the group.

In comparison to incompressible flows, data on the structure of supersonic flows are lacking, especially concerning superstructures. A review of the structure of supersonic turbulent boundary layers can be found in Smits & Dussauge (2006). Recently, Ganapathisubramani, Clemens & Dolling (2006) performed wide-field DPIV in a Mach 2 turbulent boundary layer and observed alternating streamwise structures of uniform low- and high-speed fluid in the logarithmic region with lengths exceeding their 8δ field of view.

Here we utilize a DNS database of turbulent boundary layers at a free-stream Mach number of 3. The turbulent Mach number within the boundary layer is low enough that compressibility effects are not significant, and the characteristics of the turbulence structure can be compared to those of incompressible boundary layers. We use streamwise domain lengths of $L_x = 9.1\delta$, 24δ, and 48δ, and demonstrate that in all cases the numerical data exhibit large-scale coherent structures that have been observed experimentally. Direct numerical simulation is a powerful tool for determining flow structure, and it is critical that the simulations produce realistic physics. We investigate the occurrence of low-speed superstructures in the logarithmic

Case	M_δ	ρ_δ (kg m^{-3})	T_δ (K)	T_w/T_δ	Re_θ	θ(mm)	H	δ(mm)
L09	2.98	0.0907	219.55	2.58	2390	0.430	5.4	6.04
L24	2.92	0.0750	107.80	2.85	2630	0.435	5.4	6.50
L48	2.92	0.0750	107.80	2.85	2590	0.560	5.5	6.50

TABLE 1. Dimensional boundary-layer-edge and wall parameters for the DNS. Re_θ, θ, H, and δ are defined at the inlet.

Case	δ^+	L_x/δ	L_y/δ	L_z/δ	Δx^+	Δy^+	N_x	N_y	N_z
L09	325	9.1	2.3	13.8	8.0	3.0	384	256	106
L24	420	24.0	2.2	9.0	9.3	5.8	1080	160	112
L48	480	48.0	2.2	9.0	9.3	5.8	2160	160	112

TABLE 2. Grid resolution and domain size for the DNS.

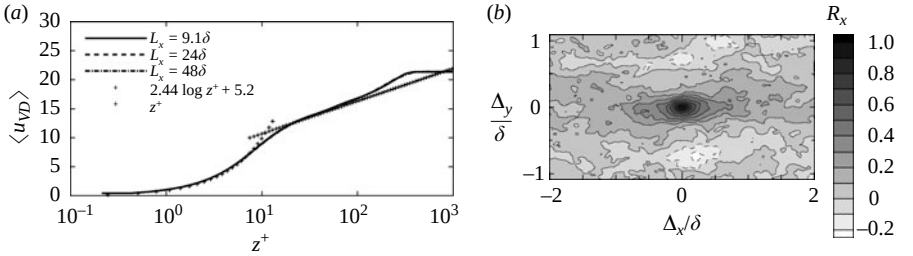

FIGURE 1. DNS statistics. (*a*) Mean velocity profiles. (*b*) Two-point correlation of the streamwise fluctuating mass flux, $R_{(\rho u)'(\rho u)'}$, at $z/\delta = 0.2$ for $L_x = 48\delta$.

region, and characterize the properties of hairpin vortex packets. Additionally, we examine the connection among hairpin packets, wall shear stress, and superstructures.

2. DNS parameters and accuracy

Table 1 gives the boundary-layer-edge conditions for the DNS, the momentum thickness, θ, shape factor, H, Reynolds number, Re_θ, and δ. The wall is isothermal, with T_w set to near the adiabatic wall temperature. Table 2 provides the grid resolution and domain size for the simulations, as well as the ratio of δ to the wall unit, δ^+. The streamwise, spanwise, and wall-normal directions are x, y, and z, respectively. Details regarding the numerical method are provided in Martín (2007), which also describes the accuracy of the DNS statistics as compared to theory and experiments. Figure 1(*a*) plots the van Driest transformed velocity profiles, showing good agreement between the prediction and the simulations. The skin friction coefficients for the $L_x = 9.1\delta$, 24δ, and 48δ cases are 0.0021, 0.0019, and 0.0018, respectively, which fall within 6% of the van Driest II prediction.

3. Results and comparison with experiments

3.1. *Two-point correlations*

For comparison with previous experiments, we compute two-point spatial correlations $R_{(\rho u)'(\rho u)'}$ of the streamwise fluctuating mass flux. Experiments report correlations of

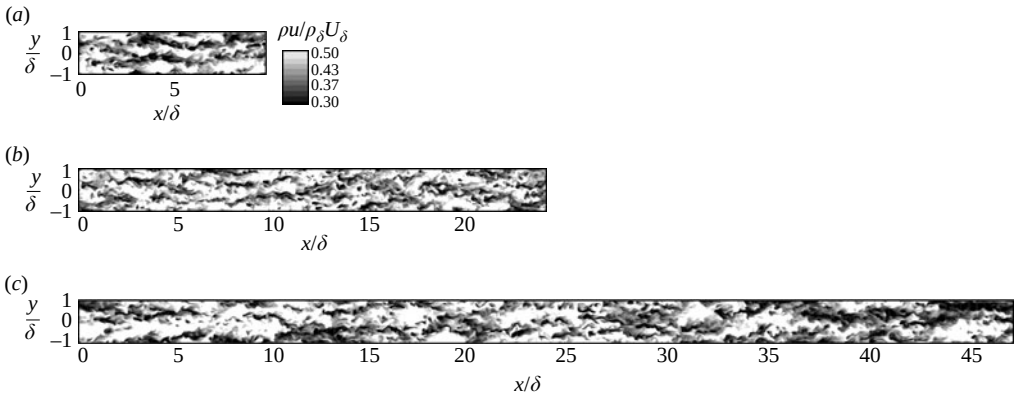

FIGURE 2. Instantaneous contours of ρu from the DNS, highlighting the low-momentum superstructures in the logarithmic region (given by the darker levels). (*a*) $L_x = 9.1\delta$; (*b*) $L_x = 24\delta$; (*c*) $L_x = 48\delta$. The planes are located at $z/\delta = 0.2$ and plotted with an x-to-y ratio of 1; the legend is the same for all data sets.

velocity only, but at Mach 3 the DNS correlations of $(\rho u)'$ and u' are very similar. We perform the correlation in (x, y)-planes of the $L_x = 48\delta$ DNS by considering 'origin' points along the mid-span line ($y = 0$) and correlating them with neighbouring points lying within a $4\delta \times 2.2\delta$ streamwise/spanwise window. The operation is done in 12 spatially independent windows for 30 time realizations separated by $5\delta/U_\delta$, yielding a total of 360 samples. The flow structures travel about 3.7δ during the $5\delta/U_\delta$ interval, assuming a convection velocity equal to the packet velocity from § 3.3. Figure 1(*b*) shows the correlation map at $z/\delta = 0.2$, within the logarithmic layer. We find elongated positive coherence in the streamwise direction, extending from the origin to about $\pm 1\delta$ at a contour level of 0.2, with spanwise-adjacent regions of negative correlation (dashed contours). At the same contour level, the structure width (span) is about 0.4δ. The DNS correlation map is similar to those reported by Hutchins & Marusic (2007*a*) and Ganapathisubramani *et al.* (2006), and consistent with the alternating structures of low- and high-speed flow observed in both the DNS and the experiments.

3.2. *Large-scale low-speed structures*

Plotting instantaneous contours of ρu in the log-law region of the DNS reveals low-momentum superstructures similar to those found in previous experiments. Figure 2 gives contour plots for the three cases in (x, y)-planes located at $z/\delta = 0.2$. The visualizations show long low-speed structures (indicated by the darker contour levels) about $(5\text{–}10)\delta$ in length that exhibit significant meandering in the spanwise direction. Many of these structures have small streamwise 'gaps' (less than 0.4δ, cf. § 4) between them and spanwise alignment such that they appear to be part of even longer structures.

To establish the importance of the low-speed structures to the overall turbulence, we compute their contribution to the turbulent kinetic energy. We consider (x, y)-planes at three wall-normal locations, $z^+ = 5$ and 15, and $z/\delta = 0.2$, and identify the structures by stipulating that u' be less than a threshold. The thresholds at each height are $-0.05\overline{u(z)}$, $-0.10\overline{u(z)}$, and $-0.05\overline{u(z)}$, respectively. We calculate the u-spectra in

Location	$L_x = 9.1\delta$	$L_x = 24\delta$	$L_x = 48\delta$
$z^+ = 5$	24.6%	23.2%	22.5%
$z^+ = 15$	37.0%	36.7%	35.9%
$z/\delta = 0.2$	36.8%	38.4%	37.9%

TABLE 3. Percentage of energy contained in the low-speed superstructures at different wall-normal locations for the DNS.

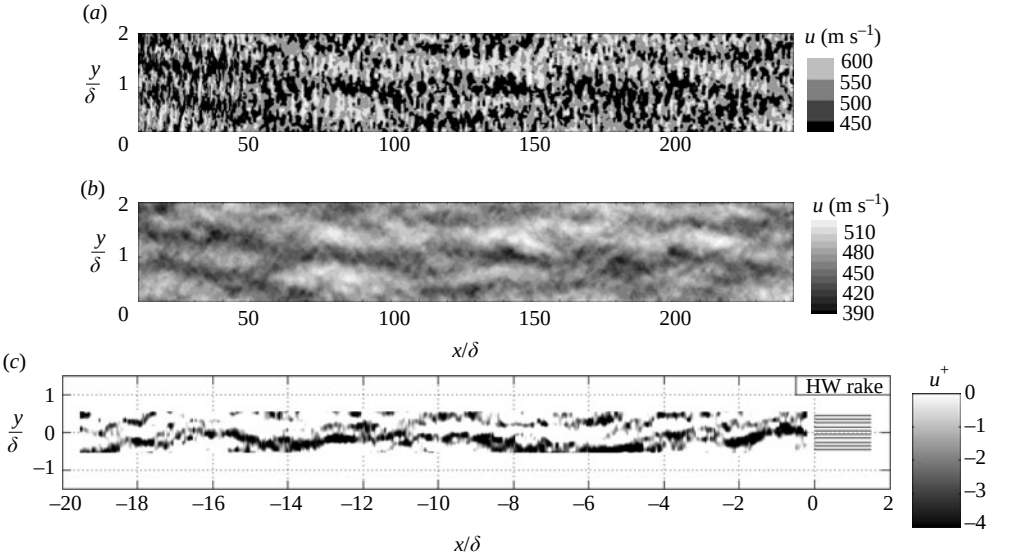

FIGURE 3. Map of u at $z/\delta = 0.2$ from DNS compared with the experimental results of Hutchins & Marusic (2007). The x-axis is reconstructed using Taylor's hypothesis; for the DNS a convection velocity based on U_δ ($\overline{U}_{0.2\delta} = 0.76U_\delta$) is used. (*a*) Raw data; (*b*) averaged in x over 4δ; (*c*) log region data from a rake of 10 hot-wire probes, adapted from Hutchins & Marusic (2007).

each plane with the velocity at non-structure points set to zero, then integrate it to obtain the energy. Table 3 gives the low-speed structure energy as a percentage of the total for each domain length. We find that the energy content does not change significantly with L_x. The low-speed structures contain about 23% of the streamwise turbulence energy at $z^+ = 5$, and over one-third of the energy at the buffer region and logarithmic layer locations.

To determine the streamwise extent of the low-speed structures, we generated a long-domain velocity map using Taylor's hypothesis of 'frozen' convection. For the shortest domain size, we ran the DNS for 300 convective time scales (δ/U_δ), and sampled the streamwise velocity at $x = 4\delta$ with a period of δ/U_δ. The data were sampled at a wall-normal location of $z/\delta = 0.2$, and the time coordinate was converted into distance using a convection velocity of $0.76U_\delta$. The streamwise sample spacing is therefore 0.76δ, which has the effect of smoothing over the small streamwise 'gaps' between the $(5–10)\delta$ structures so that any longer structures they may be a part of become visible. Figure 3(*a*) gives the resulting reconstructed velocity map, which contains long regions of low streamwise velocity, consistent with the instantaneous

contour plots shown in figure 2. These low-speed features are more evident when the higher frequency spanwise-oriented 'ripples' due to the sampling rate are removed by taking the streamwise average of u over $x = 0$–4δ at each time sample (figure 3b).

Figure 3(c) shows a similar u-contour map from Hutchins & Marusic (2007a), generated at $z/\delta = 0.15$ using a spanwise rake of 10 hot-wire probes along with Taylor's hypothesis. The boundary layer is subsonic with $Re_\tau = 14\,380$, and the data were reconstructed using a convection velocity equal to the local mean; note that the effective streamwise length of the map is 20δ. Both the DNS and experimental data contain long low-speed streamwise structures separated by regions of high velocity. One such structure extends beyond the 20δ-domain of the experiment. The DNS data show low-speed superstructures with length of order 100δ. We find that the width of the superstructures for both studies is comparable, and that their spanwise spacing is about 0.5δ. The velocity maps show that the low-speed structures of the experiments and simulations exhibit significant spanwise meandering. This was shown by Hutchins & Marusic (2007a) to cause two-point correlations to significantly underpredict the structure length, which probably accounts for the comparatively small streamwise length scale obtained from figure 1(b).

3.3. *Hairpin packets*

Inspection of the DNS data in streamwise, wall-normal planes commonly reveals hairpin packet 'signatures' as described by Adrian *et al.* (2000). We devised a post-processing code to find the packets and characterize their properties. The scheme searches (x, z)-planes for transverse, or 'head', vortices that are grouped together in the streamwise direction and form a ramp with a shallow, downstream angle relative to the wall.

We chose the swirling strength, λ_{ci}, to visualize the three-dimensional hairpin structures. The swirling strength distinguishes between vorticity coinciding with the rotating flow of compact vortices and that dominated by shear (Zhou *et al.* 1999). The packet-finding algorithm first identifies hairpin head vortices using the criteria that λ_{ci} must be greater than $4.5\overline{\lambda_{ci}}$ (where the overbar indicates the mean) and that the out-of-plane vorticity is larger than 2 standard deviations from the mean; only the region between the buffer layer ($z^+ = 30$) and the boundary layer edge is considered for both determining the threshold values and searching for hairpin packets. These criteria occasionally pick out hairpin 'legs', or tall vortical structures, that may or may not be attached below a hairpin head. The algorithm uses a maximum head-vortex size criterion, $0.1\delta \times 0.1\delta$, and categorizes larger structures as legs. It then checks for a head above the leg by testing whether the location of maximum λ_{ci} is within 0.1δ (the head size) from the top of the leg. If a head is found, only the head region is kept; otherwise, the structure is discarded. Next, the location of the core of each vortex is determined by assuming that it coincides with the local maximum of λ_{ci}. For each (x, z)-plane considered, the algorithm starts by choosing the vortex core that is closest to the location ($x = 0$, $z^+ = 30$) as the reference head for the first packet. It then searches for the next downstream vortex that is both within a streamwise distance of 0.5δ and at an angle of between 0° and 45° (with respect to the wall) from the reference vortex. If a vortex satisfying these criteria is found, it is considered to be part of a hairpin packet with the reference hairpin head, and is taken as the new reference vortex. The process continues until no new vortices belonging to the first packet are found. New packets are searched for in the same manner, until all identified vortices in the (x, z)-plane are accounted for. It should be mentioned that

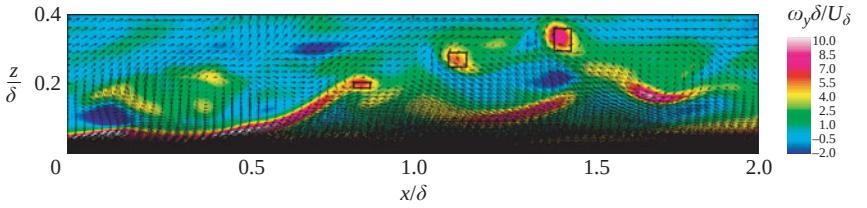

FIGURE 4. An (x, z)-plane from the DNS, $L_x = 9.1\delta$, containing a hairpin packet. Contours show spanwise vorticity, vectors give velocity with $0.69U_\delta$ subtracted from u to highlight vortical motion. Black 'boxes' mark hairpin heads identified by the packet-finding algorithm.

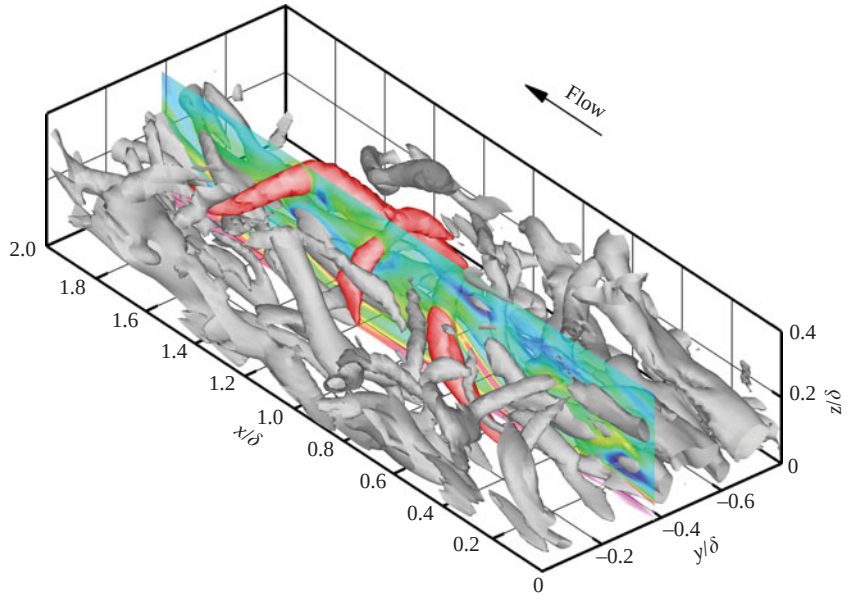

FIGURE 5. Hairpin packet from figure 4 visualized using an iso-surface of $\lambda_{ci} = 3.5\overline{\lambda_{ci}}$. The (x, z)-plane data of figure 4 are included at 50% translucency for reference. Portions of the packet hairpins not obscured by the reference plane have been coloured red.

the packet-finding algorithm searches only for vortex groups that conform to the idealized packet model (Adrian *et al.* 2000).

Figure 4 shows a typical packet found by the algorithm in an (x, z)-plane. Visualizing the identified structures in three dimensions using an iso-surface of λ_{ci} verifies that the planar vortices correspond to asymmetric cane- and horseshoe-like hairpins (see figure 5).

Once any hairpin packets are identified, we determine the packet angle, α, by calculating the arctangent of the slope of the least-squares fit through the packet vortex cores. We compute the packet convection velocity, U_{cp}, as the average streamwise velocity of the data points comprising each packet vortex. The average packet length, δ_x, height from the wall, δ_z, and streamwise head spacing, L_h, are computed from the packet vortex core positions. We generate statistics on the average packet properties by considering data in two (x, z)-planes separated by a spanwise distance of 0.75δ, so that the evaluated structures do not overlap. The results are averaged over multiple time realizations.

Case	δ_x (δ)	δ_z (δ)	α (°)	U_{cp}/U_δ	Heads	L_h ($^+$, δ)
AMT	1.3	0.8(max)	12†	0.6–0.8	2–10	139, 0.17‡
GLM	$\geqslant$2(max)	0.2(max)	NA	-	2–5¶	NA
L09	0.39	0.31	20.0	0.70	2	49, 0.15
L24	0.38	0.30	18.4	0.74	2	63, 0.15
L48	0.37	0.31	17.4	0.74	2	77, 0.16

† $Re_\theta = 7705$
‡ $Re_\theta = 2370$, $\delta^+ = 836$
¶ leg pairs in (x, y)-planes

TABLE 4. Average hairpin packet properties for the DNS, compared with data from Adrian *et al.* (2000) (AMT) and Ganapathisubramani *et al.* (2003) (GLM); see text for definitions.

Table 4 gives the average hairpin packet properties for each domain length, along with the incompressible results of Adrian *et al.* (2000) at Re_θ from 930 to 7705 and Ganapathisubramani *et al.* (2003) at $Re_\theta = 2500$, which is comparable to the DNS. For the results of Adrian *et al.* (2000) the values listed are representative of the data as a whole, unless otherwise indicated by footnotes. We find that the packet properties for the DNS do not vary significantly with domain length. The apparently shorter length of the supersonic packets compared to the subsonic cases can be explained as follows. The value of 1.3δ reported by Adrian *et al.* (2000) is for $Re_\theta = 7705$ data, in which packets may contain more than 10 hairpins (the number of hairpins was observed to increase with Re_θ), making them much longer than the average DNS packet. Although Ganapathisubramani *et al.* (2003) found packets of length greater than 2δ, the average packet length is not definitive due to uncertainties arising from their feature-extraction algorithm. The most that can be said is that it is less than 2δ. In general, table 4 shows that the packet characteristics are similar for the subsonic and supersonic cases. For example, the average number of hairpins per packet for the DNS is within the range reported by Ganapathisubramani *et al.* (2003) (the range for the DNS is 2–6 hairpin heads), and is in agreement with that given by Adrian *et al.* (2000) at low Reynolds numbers. It is presently unclear if the disagreement in α between the DNS data and those of Adrian *et al.* (2000) is due to the Reynolds number difference, a compressibility effect, or other factors. The α reported by Adrian *et al.* (2000) was for their highest Re_θ and computed without regard to each packet's wall-normal location, consistent with the present study. However, Adrian *et al.* (2000) observed an increase in α with z, so that care must be taken when making comparisons. The DNS α lies within the range measured by Adrian *et al.* (2000), and is close to the value of 20° given by Head & Bandyopadhyay (1981) at Re_θ of order 10 000.

We investigate the connection between hairpin packets and the wall shear stress, τ_w, by correlating τ_w and u using the method of Brown & Thomas (1977), and assuming that the ramp-like structures they identified were hairpin packets. For each wall-normal location, the correlation is defined as:

$$R_{\tau_w u}(\Delta x) = \left\langle \overline{\int_{x_1}^{x_2} \tau_w'(x) u'(x + \Delta x)\, \mathrm{d}x} \right\rangle / \tau_{w,RMS}' u_{RMS}'.$$

Figure 6(a) plots $R_{\tau_w u}$ at different wall-normal locations. The correlation peaks at increasing Δx as the velocity is measured farther away from the wall. Figure 6(b) plots the 'enhanced' correlation. The enhanced correlation is obtained by conditionally

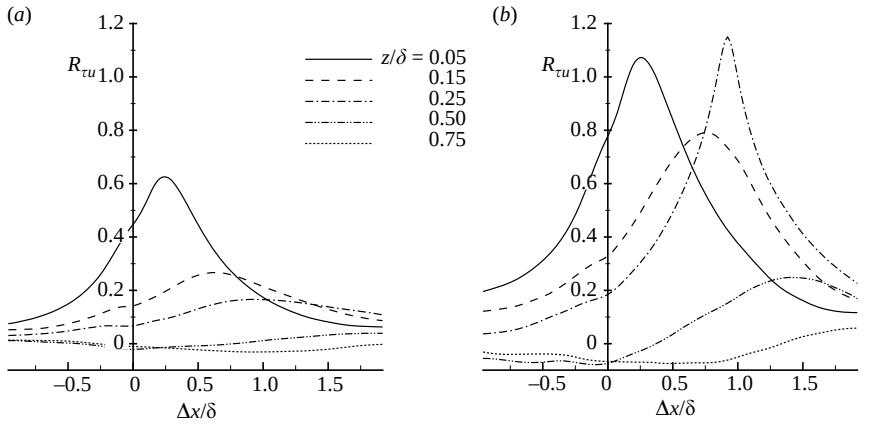

FIGURE 6. Time-averaged spatial correlations between τ_w and u versus streamwise distance at different wall-normal locations: (a) standard correlation; (b) 'enhanced' correlation.

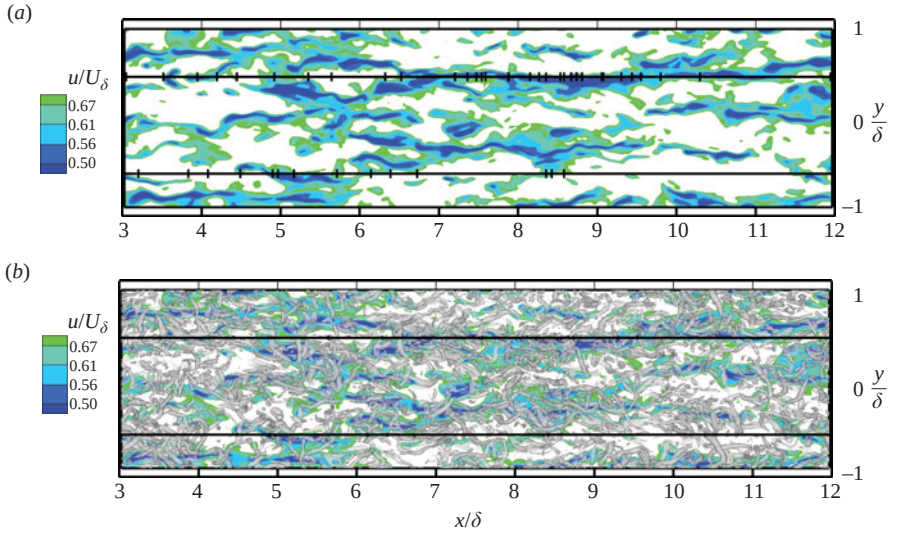

FIGURE 7. Instantaneous visualization connecting the large-scale low-speed regions with hairpin packets; see text for description.

averaging the instances in which the correlation at $z/\delta = 0.25$ is greater than 0.3 at the peak Δx location shown in figure 6(a). The result is a correlation of the same shape as that given in figure 6(a) with a much greater amplitude at different wall-normal locations. According to Brown & Thomas (1977), this is evidence for the existence of some organized structure. The angle of the structure is computed by a least-squares fit of the peak points at z/δ from 0.05 to 0.5 in figure 6(b), which gives a value of about 21°. This is consistent with the angle given by the hairpin-packet-searching algorithm, so it is likely that there is a connection between hairpin packets and τ_w.

4. Very large-scale motions

To determine if the DNS data support the VLSM model proposed by Kim & Adrian (1999), we created instantaneous visualizations of the flow structure augmented by the

packet-finding algorithm. Figure 7 shows a 9δ-long flow volume extracted from the $L_x = 24\delta$ DNS and viewed from above, i.e. facing the (x, y)-plane. Colour contours of u are given in an (x, y)-plane at the top of the buffer region ($z^+ = 30$); to highlight the low-speed structures, only values less than U_{cp} are shown. In figure 7(a) two vertical, or (x, z)-plane, 'slices' of data are represented by horizontal black lines at $y = 0.52\delta$ and -0.68δ, respectively. The first slice was chosen because much of it is intersected by a low-speed structure, while the second slice is located primarily in a region of high-speed flow. Tick marks along each horizontal line give the streamwise core locations of hairpin packet vortices found by applying the algorithm described above in the selected (x, z)-planes. Figure 7(a) shows that these vortices are concentrated predominantly where the zones of low-speed fluid intersect the vertical slices chosen, so that the (x, z)-plane at $y = 0.52\delta$ contains a much higher number of packet vortices than the slice at $y = -0.68\delta$. Figure 7(b) provides an instantaneous visualization of the hairpin vortex structures for the same volume using an iso-surface of λ_{ci} at a value of $3.5\overline{\lambda_{ci}}$; the iso-surface is plotted at 40% translucency so that the u-contours are visible behind it. Consistent with the data of figure 7(a), figure 7(b) shows symmetric and asymmetric hairpin vortices clustered primarily above the low-speed superstructures. This lends support to the VLSM model of Kim & Adrian (1999).

The low-speed superstructures described above are highly three-dimensional, appearing as chains of 'bulges' when viewed using an iso-surface of streamwise velocity. Therefore, visualizing them in (x, y)-planes (cf. figure 2) may show small streamwise 'gaps' filled with high-speed fluid existing along them. The planar images of figure 2 show that the 'gaps' between many of the $(5–10)\delta$-long structures are less than the average packet length, and could indicate the high-speed regions between successive 'bulges' or packets. Therefore, these $(5–10)\delta$ features may be part of even longer superstructures, as illustrated by the visualization using Taylor's hypothesis (figure 3b).

5. Concluding remarks

We utilize a DNS database of Mach 3 turbulent boundary layers and show that the numerical data contain the same large-scale coherent structures observed in experiments at both supersonic and incompressible conditions. Contours of the instantaneous mass flux from the $L_x = 9.1\delta$, 24δ, and 48δ DNS indicate long low-momentum superstructures that exhibit significant spanwise meandering, consistent with previous experiments. These structures are found to carry about one-third of the total turbulent kinetic energy. Using Taylor's hypothesis allows the reconstruction of a streamwise velocity map in the logarithmic region having a domain length of 230δ. Even using the shortest computational domain size, the map shows superstructures that attain lengths of order 100δ. The spanwise meandering of these structures is the most likely reason for the discrepancy between their observed length and that obtained from the mass-flux correlations, as this meandering would effectively mask the structures from two-point statistical methods (see Hutchins & Marusic 2007a). A hairpin-packet-finding algorithm is used to determine the average properties of the DNS packets. The results show that the Mach 3 packets are similar to those measured at incompressible conditions. We employ the enhanced correlation technique of Brown & Thomas (1977) and find a connection between hairpin packets and the wall shear stress. Visualization of the instantaneous, three-dimensional turbulence structure shows streamwise groups of hairpin packets that are concentrated predominantly

above the low-speed superstructures. This is consistent with the VLSM model proposed by Kim & Adrian (1999).

We would like to acknowledge the support from the Air Force Office of Scientific Research under grant no. AF/F49620-02-1-0361 and the National Science Foundation under grant no. CTS-0238390.

REFERENCES

Adrian, R., Meinhart, C. & Tomkins, C. 2000 Vortex organization in the outer region of the turbulent boundary layer. *J. Fluid Mech.* **422**, 1–54.

del Álamo, J. C. & Jiménez, J. 2003 Spectra of the very large anisotropic scales in turbulent channels. *Phys. Fluids* **15** (6), L41–L44.

del Álamo, J. C., Jiménez, J., Zandonade, P. & Moser, R. D. 2004 Scaling of the energy spectra of turbulent channels. *J. Fluid Mech.* **500**, 135–144.

del Álamo, J. C., Jiménez, J., Zandonade, P. & Moser, R. D. 2006 Self-similar vortex clusters in the turbulent logarithmic region. *J. Fluid Mech.* **561**, 329–358.

Balakumar, B. J. & Adrian, R. J. 2007 Large- and very-large-scale motions in channel and boundary-layer flows. *Phil. Trans. R. Soc. Lond.* A **365**, 665–681.

Brown, G. L. & Thomas, A. S. W. 1977 Large structure in a turbulent boundary layer. *Phys. Fluids* **10**, 243–251.

Delo, C. J., Kelso, R. M. & Smits, A. J. 2004 Three-dimensional structure of a low-Reynolds-number turbulent boundary layer. *J. Fluid Mech.* **512**, 47–83.

Ganapathisubramani, B., Clemens, N. & Dolling, D. 2006 Large-scale motions in a supersonic turbulent boundary layer. *J. Fluid Mech.* **556**, 1–11.

Ganapathisubramani, B., Longmire, E. K. & Marusic, I. 2003 Characteristics of vortex packets in turbulent boundary layers. *J. Fluid Mech.* **478**, 35–46.

Guala, M., Hommema, S. E. & Adrian, R. J. 2006 Large-scale and very-large-scale motions in turbulent pipe flow. *J. Fluid Mech.* **554**, 521–542.

Hambleton, W. T., Hutchins, N. & Marusic, I. 2006 Simultaneous orthogonal-plane particle image velocimetry measurements in a turbulent boundary layer. *J. Fluid Mech.* **560**, 53–64.

Head, M. & Bandyopadhyay, P. 1981 New aspects of turbulent boundary-layer structure. *J. Fluid Mech.* **107**, 297–338.

Hutchins, N. & Marusic, I. 2007*a* Evidence of very long meandering features in the logarithmic region of turbulent boundary layers. *J. Fluid Mech.* **579**, 1–28.

Hutchins, N. & Marusic, I. 2007*b* Large-scale influences in near-wall turbulence. *Phil. Trans. R. Soc. Lond.* A **365**, 647–664.

Jiménez, J. 1998 The largest scales of turbulent wall flows. In *Center for Turbulence Research, Annual Research Briefs*, pp. 137–154. Stanford University.

Kim, K. C. & Adrian, R. J. 1999 Very large-scale motion in the outer layer. *Phys. Fluids* **11**, 417–422.

Martín, M. P. 2007 Direct numerical simulation of hypersonic turbulent boundary layers. Part 1: initialization and comparison with experiments. *J. Fluid Mech.* **570**, 347–364.

Smits, A. J. & Dussauge, J.-P. 2006 *Turbulent Shear Layers in Supersonic Flow*, 2nd edn. Springer.

Theodorsen, T. 1952 Mechanism of turbulence. In *Proc. 2nd Midwestern Conf. on Fluid Mech.*, pp. 1–19. Ohio State University, Columbus, Ohio, USA.

Tomkins, C. & Adrian, R. 2003 Spanwise structure and scale growth in turbulent boundary layers. *J. Fluid Mech.* **490**, 37–74.

Zhou, J., Adrian, R., Balachandar, S. & Kendall, T. 1999 Mechanisms for generating coherent packets of hairpin vortices in channel flow. *J. Fluid Mech.* **387**, 353–396.